DMD Fast Forward. Published on November 15, 2018 as DOI: 10.1124/dmd.118.084459
This article has not been copyedited and formatted. The final version may differ from this version.

Bioavailability, Biotransformation, and Excretion of the Covalent BTK Inhibitor Acalabrutinib in Rats, Dogs, and Humans

Terry Podoll, Paul G. Pearson, Jerry Evarts, Tim Ingallinera, Elena Bibikova, Hao Sun, Mark Gohdes, Kristen Cardinal, Mitesh Sanghvi, and J. Greg Slatter

Acerta Pharma, South San Francisco, California (TP, JE, TI, EB, JGS)

Pearson Pharma Partners, Westlake Village, CA (PGP)

Covance, Madison, Wisconsin (HS, MG, KC)

Xceleron, Germantown, Maryland (MS)

DMD Fast Forward. Published on November 15, 2018 as DOI: 10.1124/dmd.118.084459
This article has not been copyedited and formatted. The final version may differ from this version.

a) Bioavailability, Metabolism, and Excretion of [^{14}C]Acalabrutinib

b) Terry Podoll, PhD, 5021 Bowen Place S, Seattle, WA 98118,

voice: 402-500-0573,

fax: 206-374-2788,

email: terry.podoll@iv-po.com

c) Number of text pages: 54

Number of tables: 5

Number of figures: 4

Number of references: 26

Number of words in the Abstract: 235/250

Number of words in the Introduction: 566/750

Number of words in the Discussion: 1603/1500

d) List of nonstandard abbreviations (alphabetical order):

Abbreviations: ADME, absorption, distribution, metabolism, and excretion; AMS, accelerator mass spectrometry; $AUC_{0\text{-}12h}$, area under the plasma concentration-time curve from 0 hour to 12 hours; $AUC_{0\text{-}168h}$, AUC from 0 hour to 168 hours; $AUC_{0\text{-}\infty}$, AUC from time 0 to infinity (ng equivalent hours/g); $AUC_{0\text{-}t}$, area under the concentration time curve from time 0 to the last quantifiable concentration (ng equivalent hours/g); BTK, Bruton tyrosine kinase; CL, clearance; CLR renal CL; C_{max}, maximum concentration (ng equivalent/g); CV, coefficient of variation; CYP, cytochrome P450; CYP3A, cytochrome P450 3A; F, bioavailability fraction of dose absorbed relative to IV dosing expressed as a percent; $\%f_{eu}$, percent excreted in urine over the sample collection period; FBS, fetal bovine serum; FDA, Food and Drug Administration; GSH, glutathione; HPLC, high-performance liquid chromatography; LC-MS/MS, liquid chromatography-tandem mass spectrometry; LSC, liquid scintillation counting; MS, mass spectrometry;

DMD Fast Forward. Published on November 15, 2018 as DOI: 10.1124/dmd.118.084459
This article has not been copyedited and formatted. The final version may differ from this version.

ND, not determined; NA, not applicable - entire profile not detectable; NC, not calculated due to the lack of a distinct elimination phase; NC1, not calculated due to less than 3 available concentration values; NC2, not calculated due to the lack of a distinct elimination phase; PBMC, peripheral blood mononuclear cell; PK, pharmacokinetics; $t_{1/2}$, half-life; TCI, targeted covalent inhibitor; T_{max}, time of maximum observed plasma concentration; V_{ss}, V_z at steady state; V_z, volume of distribution.

DMD Fast Forward. Published on November 15, 2018 as DOI: 10.1124/dmd.118.084459
This article has not been copyedited and formatted. The final version may differ from this version.

Abstract

Acalabrutinib is a targeted, covalent inhibitor of Bruton tyrosine kinase (BTK) with a unique 2-butynamide warhead that has relatively lower reactivity than other marketed acrylamide covalent inhibitors. A human [^{14}C] microtracer bioavailability study in healthy subjects revealed moderate intravenous clearance (39.4 l/h) and an absolute bioavailability of 25.3 ± 14.3% (*N* = 8). Absorption and elimination of acalabrutinib following a 100 mg [^{14}C] microtracer acalabrutinib oral dose were rapid, with maximum concentration reached in <1 h and elimination half-life values <2 h. Low concentrations of radioactivity persisted longer in the blood cell fraction and a peripheral blood mononuclear cell (PBMC) subfraction (enriched in target BTK) relative to plasma. [^{14}C]acalabrutinib was metabolized to over three dozen metabolites detectable by liquid chromatography-tandem mass spectrometry (LC-MS/MS), with primary metabolism by cytochrome P450 (CYP) 3A-mediated oxidation of the pyrrolidine ring, thiol conjugation of the butynamide warhead, and amide hydrolysis. A major active, circulating, pyrrolidine ring-opened metabolite, ACP-5862, was produced by CYP3A oxidation. Novel enol thioethers from the 2-butynamide warhead arose from glutathione and/or cysteine Michael additions and were subject to hydrolysis to a β-ketoamide. Total radioactivity recovery was 95.7 ± 4.6% (*n* = 6), with 12.0% of dose in urine and 83.5% in feces. Excretion and metabolism characteristics were generally similar in rat and dog. Acalabrutinib's highly selective, covalent mechanism of action, coupled with rapid absorption and elimination, enables high and sustained BTK target occupancy following twice daily administration.

Introduction

Acalabrutinib (CALQUENCE®) is a highly selective, potent, orally administered, targeted covalent inhibitor (TCI) of Bruton tyrosine kinase (BTK) that received accelerated approval for relapsed/refractory mantle cell lymphoma by the United States Food and Drug Administration (FDA) in October 2017 (Wang et al., 2018). BTK is a Tec family kinase expressed in B cells, myeloid cells, mast cells, and platelets, which plays an integral role in B-cell receptor signaling that is responsible for the proliferation and survival of malignant B cells (Buggy and Elias, 2012). Irreversible inactivation of BTK was established as a valuable clinical target for the treatment of B-cell malignancies by the first-in-class agent, ibrutinib (Ponader and Burger, 2014). Adverse effects of ibrutinib therapy include bleeding and atrial fibrillation, which were postulated to involve off-target activity against other Tec (Wang, et al., 2018) and Src (Barf, et al., 2017) family kinases. The discovery and development of acalabrutinib focused on reducing overall warhead reactivity and improving selectivity for BTK (Barf, et al., 2017).

Recent regulatory approvals of TCIs of other protein kinases have led to interest in identifying desirable physicochemical and absorption, distribution, metabolism, and excretion (ADME) properties in drug candidates (Liu et al. 2013; Moghaddam et al., 2014; Baillie, 2016; Lonsdale and Ward, 2018). Unlike drugs that interact reversibly with their targets and generally require sustained systemic exposure to achieve target coverage over the dose interval, potent TCIs can drive high target occupancy after a relatively brief systemic exposure. This can result in prolonged pharmacodynamic effects, with the duration of effect related to the time required for target resynthesis. (Singh et al., 2011; Barf and Kaptein, 2012).

Prior to acalabrutinib, clinically approved protein kinase TCIs included ibrutinib (BTK), osimertinib (epidermal growth factor receptor), neratinib (human epidermal growth factor receptor 2 [HER2]), and afatinib (HER1, HER2, and HER4). While targeting distinct protein kinases, all four of these agents employ an electrophilic acrylamide warhead that targets a selected cysteine thiol nucleophile in the ATP binding pocket of each protein kinase. The acrylamide functionality has been used more than any other electrophilic warhead in the development of TCIs of protein kinases (Zhao and Bourne, 2018). They have the advantage of high potency against their respective protein kinase targets, however can lack kinase selectivity and result in off-target binding to plasma proteins (Chandrasekaran et al. 2010; Stopfer et al., 2012; Scheers et al., 2015; Dickinson et al., 2016). Osimertinib covalent plasma protein binding is extensive enough to suggest it provides a significant route of clearance (Dickinson et al., 2016). Glutathione (GSH) conjugation of the acrylamide warhead is a metabolic route of approved TCIs (Shibata and Chiba, 2015).

Acalabrutinib contains a 2-butynamide electrophilic warhead that is less reactive than an analogue with the corresponding acrylamide warhead (Barf et al., 2017). The cysteine-481 target nucleophile in BTK has a proximal asparagine residue that lowers the pK_a of the cysteine-481 thiol, thereby increasing its nucleophilicity. This results in improved selectivity (Barf et al. 2017) and the metabolic fate of this functional group has not been previously described.

Initial clinical studies indicate that acalabrutinib has optimal characteristics of a TCI, namely rapid absorption, low systemic exposure, and a short plasma half-life. This results in high and sustained selective BTK occupancy and durable clinical effectiveness with twice daily dosing (Byrd et al., 2016; Barf et al., 2017, Wang et al., 2018). Reported here are the ADME properties of [^{14}C]acalabrutinib in rats, dogs, and humans.

DMD Fast Forward. Published on November 15, 2018 as DOI: 10.1124/dmd.118.084459
This article has not been copyedited and formatted. The final version may differ from this version.

Materials and Methods

Radiolabeled Acalabrutinib and Reference Standards. [^{14}C]acalabrutinib (1,4-[8-amino-3-[(2S)-1-but-2-ynoylpyrrolidin-2-yl]imidazo[1,5-α]pyrazin-1-yl]-*N*-(2-pyridyl)-benzamide) was labeled in the carbonyl carbon atom of the 2-pyridylbenzamide moiety (Fig. 1), with specific activity 57 mCi/mmol. Metabolite standards were prepared by Kalexsyn (Kalamazoo, MI) or Acerta Pharma, BV (Oss, Netherlands; data on file).

Reversible Plasma Protein Binding and Red Blood Cell Partitioning. Prior to conducting plasma incubations, nonspecific binding to the low-binding polycarbonate tubes (Sumitomo Bakelite, Akita, Japan) by both acalabrutinib and ACP-5862 were determined in phosphate buffered saline using LC-MS/MS. Additionally, the stability of acalabrutinib (1 μM) was established in potassium oxalate/sodium fluoride male mouse and rat plasma, EDTA male dog and monkey plasma, and lithium heparin male human plasma for 16 hours at 4°C using low-binding polycarbonate tubes and LC-MS/MS analysis. Then the free fraction of [^{14}C]acalabrutinib (1, 3, and 10 μM) in plasma was determined by ultracentrifugation with liquid scintillation counting (LSC) of supernatant. [^{14}C]Acalabrutinib reversible binding to pure human serum albumin solution (physiologic, 40 mg/mL) and α1-acid glycoprotein solution (physiologic, 20 μM) were determined similarly. Free fraction of the metabolite ACP‑5862 (1 and 10 μM) was determined similarly by ultracentrifugation and LC-MS/MS quantification. Red blood cell partitioning of acalabrutinib and ACP-5862 were determined following a 15-minute male whole blood incubation at 37°C and centrifugation, followed by LC-MS/MS of plasma. The radiochemical purity of [^{14}C]acalabrutinib was 96.7% 20 days before the protein binding experiments and 96.6% 23 days after using radiochromatographic analysis.

Absorption, Distribution, Metabolism, and Excretion of [^{14}C]Acalabrutinib in Rat and Dog. Pharmacokinetics (PK) and ADME of [^{14}C]acalabrutinib were characterized in male and female Sprague-Dawley rats (Hsd:Sprague Dawley SD [Envigo RMS, Inc., Indianapolis, IN], 7-8 weeks of age at dosing, *n* = 15/sex for PK, *n* = 3/sex for excreta and carcass) and Beagle dogs (Covance Research Products, Cumberland, VA, *n* = 3/sex) that had been assigned to groups and following oral administration of a 100 and 30 mg/kg dose of [^{14}C]acalabrutinib (50 and 10 μCi/kg), respectively. Whole blood, plasma, urine, and feces samples were collected at appropriate intervals through 96 hours postdose. Plasma samples were extracted twice and feces homogenates were extracted three times into methanol (sample:methanol, 1:3, v:v). For each the mixture was sonicated (10 minutes), vortexed (10 minutes), centrifuged (2400g, 10 minutes at ambient temperature), and the supernatant was separated. Following the second or third extraction the combined supernatants were reduced to dryness under a stream of nitrogen at 60°C. The extract was then reconstituted in water/methanol (70/30 v/v, 300 µL) before analysis by LC-MS and/or LC-MS/MS, with eluent fraction collection and TopCount (PerkinElmer, Waltham, MA) radioanalysis. Radiochromatographic profiles were used to identify and quantify metabolites. Whole blood and feces samples were processed by digestion and combustion, respectively, before being analyzed for total radioactivity by LSC. All preclinical work was conducted in a facility accredited by the Association for Assessment and Accreditation of Laboratory Animal Care International, in compliance with applicable animal welfare regulations and after protocol approval by its Institutional Animal Care and Use Committee.

Human [^{14}C]Acalabrutinib Microtracer Absolute Bioavailability, Metabolism, and Excretion Study. A phase 1, open-label, single-center, nonrandomized, 2-cohort study was conducted in healthy subjects. A radiolabel microtracer dose was used to determine the absolute bioavailability of acalabrutinib in participants enrolled in cohort 1

DMD Fast Forward. Published on November 15, 2018 as DOI: 10.1124/dmd.118.084459
This article has not been copyedited and formatted. The final version may differ from this version.

and to determine the mass balance for those in cohort 2. The study was performed in accordance with the ethical principles stated in the Declaration of Helsinki, FDA regulation 21 CFR, Parts 50, 56, 312, and 361.1 and International Conference on Harmonization guidelines for good clinical practice. All subjects provided informed consent on an institutional review board-approved protocol. Healthy male and female subjects aged 18–65 years were recruited at a single site (Covance Clinical Research Unit, Madison, WI). The use of prescribed or nonprescribed concomitant medications was not permitted in the 14 days or 7 days (respectively) before the first administration of acalabrutinib unless deemed acceptable by the investigator. In addition, use of any drugs known to be significant inducers or inhibitors of CYP enzymes and/or P-glycoprotein, including St. John's Wort, was not permitted for 28 days before the dose of acalabrutinib and throughout the study. Subjects were also excluded if they had consumed alcohol-, grapefruit-, or caffeine-containing food and beverages within 72 hours of the first administration of acalabrutinib. All subjects were screened within 28 days before study entry and could only participate in one cohort. Eligible subjects were admitted to the study center on day –1. Subjects fasted overnight (at least 8 hours) before administration of acalabrutinib on day 1.

Cohort 1: Absolute Bioavailability. Bioavailability of a single 100-mg dose of the oral to-be-marketed capsule formulation of unlabeled acalabrutinib was measured in male and female healthy subjects (n = 8) relative to a microtracer dose of [^{14}C]acalabrutinib (<10 μg; ≤1 μCi) administered as a 2-minute intravenous (IV) push (5 ml of an approximately 0.194 μCi/ml saline solution), timed to finish 1 hour after the unlabeled oral dose, approximating the maximum observed plasma concentration (C_{max}) reported in prior studies. Blood samples were collected at predose; 15, 30, 45, and 58 minutes (immediately before IV push); 1 hour (immediately after the end of IV push), 1 hour 5 minutes, 1 hour 10 minutes, 1 hour 15 minutes, 1 hour 20 minutes, and 1 hour 30

minutes; and at 2, 3, 4, 5, 6, 8, 12, 24, 36, 48, 60, 72, and 96 hours after the oral dose. Complete urine collections were at the following intervals: –12 to 0 (before dose, up to the last void within 20 minutes before oral dosing), 0 to 6 hours, 6 to 12 hours, 12 to 24 hours, 24 to 48 hours, and 48 to 72 hours post oral dose. Plasma and urine samples were analyzed for total acalabrutinib by LC-MS/MS, and [^{14}C]acalabrutinib was analyzed by high-performance liquid chromatography (HPLC) fractionation and accelerator mass spectrometry (AMS). The subjects were released from the clinical site following 4 days of continuous residence. The IV dose ^{14}C content for microtracer analysis by AMS represented only 0.008% w/w of the total 100 mg acalabrutinib oral dose and therefore did not meaningfully contribute to the area under the concentration-time curve (AUC) of unlabeled acalabrutinib (Sarapa et al., 2005; Lappin and Stevens, 2008).

Cohort 2: Excretion Study. A single dose of [^{14}C]acalabrutinib (100 mg) was administered as an oral solution (free base equivalent) containing a microtracer (<10 μg; ≤1 μCi [^{14}C]acalabrutinib, in 100 ml of an approximately 0.009 µCi/ml Tang Orange Drink solution) in male and female healthy subjects (n = 6). The routes and rates of excretion of [^{14}C]acalabrutinib were determined by assessment of concentrations of total ^{14}C radioactivity and of acalabrutinib and its metabolites in whole blood, plasma, and urine, as well as percentage recovery of the radioactive dose in urine and feces. Blood samples for total ^{14}C determination in whole blood and plasma and unlabeled acalabrutinib determination in plasma were collected at the following time points: predose; 15, 30, 45, 60, 75, and 90 minutes; 2 hours, 2 hours 30 minutes; and at 3, 4, 5, 6, 8, 12, 24, 48, 72, 96, 120, 144, and 168 hours postdose. Complete urine collections for unlabeled acalabrutinib and total ^{14}C determination were collected and pooled over the following intervals: –12 to 0 (before dose, up to the last void within 20 minutes before dosing), 0 to 6 hours, 6 to 12 hours, 12 to 24 hours, and at 24-hour intervals through 168 hours postdose. Complete feces collections for total ^{14}C determination were collected and

DMD Fast Forward. Published on November 15, 2018 as DOI: 10.1124/dmd.118.084459
This article has not been copyedited and formatted. The final version may differ from this version.

pooled from predose (within 24 hours of dosing; if possible), 0 to 24 hours postdose, and at 24-hour intervals through 168 hours postdose. Total ^{14}C radioactivity was also determined in peripheral blood mononuclear cells (PBMCs) from blood samples collected at the following time points: predose; 1, 12, 24, 48, and 96 hours postdose. PBMCs were isolated from heparinized whole blood samples on the day of collection using the Ficoll-Paque™ gradient purification method (GE Healthcare, Uppsala, Sweden) and cryopreserved in 90% fetal bovine serum (FBS) plus 10% DMSO. Genotype analysis was performed for select variants of breast cancer resistance protein (BCRP or ABCG2, 421C>A), CYP3A5 (6986A>G), and GSTM1 (-/- [null], -/+, +/+). The subjects resided continuously at the study center from check-in until 7 days after administration of [^{14}C]acalabrutinib.

Quantitative Bioanalysis of Human Samples. The analysis of radioactivity was performed by Xceleron Inc. by AMS (Germantown, MD). Freeze-dried feces samples were combusted in a sample oxidizer and the resulting CO_2 trapped and analyzed in a liquid scintillation counter. Whole blood, plasma, PBMCs, and urine were analyzed for ^{14}C total radioactivity using a qualified graphitization and AMS assay. Sodium benzoate was employed as a carbon carrier for PBMC and urine samples.

[^{14}C]Acalabrutinib concentrations were determined in urine and plasma samples from cohort 1 using a validated fraction collection, graphitization, and AMS analysis (HPLC+AMS assay). Following extraction (plasma only) the samples were separated using an Agilent 1200 HPLC System, equipped with UV detector and 96-well plate fraction collector and fitted with a Waters Xterra MS C8, 4.6 x 150 mm, 3.5 micron HPLC column (55°C), pumping a 10 mM ammonium bicarbonate in water, pH 9/acetonitrile gradient. The effluent was monitored at $\lambda = 230$ nm to ensure separation of [^{14}C]acalabrutinib from other metabolites, which was achieved over a 17-minute total run time.

DMD Fast Forward. Published on November 15, 2018 as DOI: 10.1124/dmd.118.084459
This article has not been copyedited and formatted. The final version may differ from this version.

Plasma and urine samples were analyzed for unlabeled acalabrutinib parent molecule by validated LC-MS/MS methods against a stable labeled internal standard at BASi (West Lafayette, IN) following protein precipitation using acetonitrile. The quantification range for acalabrutinib in lithium heparin plasma was 1–1000 ng/ml, while that in urine was 50–5000 ng/ml. The precision (%coefficient of variation [CV]) and accuracy (%bias) observed for acalabrutinib ranged from 1.1 to 3.4 and 0.9 to 2.7 in plasma; and 1.1 to 1.9 and –1.3 to –1.1 in urine, respectively.

Pharmacokinetic Analysis. Relevant pharmacokinetic parameters were determined for plasma [^{14}C]acalabrutinib (human ADME cohort 1, IV only), and acalabrutinib, and whole blood and plasma for total ^{14}C radioactivity. The analyses were performed at Covance (Madison, WI) using standard noncompartmental methods with Phoenix WinNonlin version 6.4 (Certara USA, Inc., Princeton, NJ). The AUC parameters were calculated using actual sampling times and the linear trapezoidal rule for increasing concentrations and the logarithmic rule for decreasing concentrations (linear up, log down method).

Human Mass Balance. Radioactive ^{14}C recovery in feces was calculated by summation of the amount excreted in each collection interval during the residential period up to 168 hours postdose. One subject withdrew from the study early. Total recovery of radioactivity for this subject was calculated through 72 hours where data were available. Since >90% of total radioactivity was recovered, this subject was not excluded from summary statistics for total recovery.

Human Metabolite Identification. After analysis of plasma, feces, and urine samples by AMS, or LSC for total radioactive content, appropriate samples were pooled across subjects and time points to give one plasma time-proportional pool (Hamilton et al., 1981), one urine, and one fecal sample for metabolite profile analysis at Xceleron Inc. (Germantown, MD), and one each for metabolite identification at Covance (Madison,

WI). Acalabrutinib and its metabolites were extracted twice from plasma using methanol and twice from fecal homogenate using dimethylacetamide; urine was analyzed without extraction. The metabolite profiles in pooled urine and feces were determined using HPLC-UV combined with offline radioactivity monitoring by AMS for detection/quantification, mass spectrometry (MS) for structure elucidation, and UV for retention time matching between HPLC-UV fractionation for AMS and HPLC-UV-MS systems.

Human Sample Extraction and Metabolite Identification. The pooled plasma sample was extracted by adding methanol (3000 μL) to plasma (1000 μL); the mixture was sonicated (10 minutes), vortexed (10 minutes), centrifuged (3210*g*, 10 minutes at 4°C), and the supernatant was separated. A second extraction was executed in the same way, and the combined supernatants were reduced to dryness under a stream of nitrogen at 60°C. The extract was then reconstituted in water/methanol (70/30 v/v, 500 μL), and the radioactivity measured by AMS and compared against an unextracted sample.

The cross-subject and time-pooled fecal homogenate sample (~500 mg) was mixed with dimethylacetamide (1500 µl), vortexed (5 minutes), and centrifuged (3210*g*, 10 minutes, 4°C), and supernatant was separated, a second extraction was executed in the same way, and the combined supernatants were diluted 10-fold using water. The undiluted feces extract was analyzed by LSC for radioactivity content to determine the extraction efficiency. Diluted sample extracts were also vortexed and analyzed by HPLC-AMS; and HPLC-MS/MS.

The pooled urine sample was directly subjected to chromatographic separation by HPLC-AMS and HPLC-MS/MS analysis.

Following extraction (plasma only) the rat, dog, and human samples were separated using a Shimadzu/Prominence HPLC System, coupled with a Thermo Fisher Scientific Q Exactive mass spectrometer and fitted with a Waters Xterra MS C8, 4.6 x 150 mm, 5

micron HPLC column (55°C), pumping a 10 mM ammonium bicarbonate in water, pH 9/acetonitrile gradient. Separation was achieved over a 66-minute total run time.

DMD Fast Forward. Published on November 15, 2018 as DOI: 10.1124/dmd.118.084459
This article has not been copyedited and formatted. The final version may differ from this version.

Results

Reversible Plasma Protein Binding and Red Blood Cell Partitioning. The stability and nonspecific binding of acalabrutinib and major active circulating metabolite ACP‑5862 (BTK IC_{50} = 5.0 nM in a biochemical kinase assay, see Multi-disciplinary Review available at https://www.accessdata.fda.gov/drugsatfda_docs/nda/2017/210259Orig1s000MultidisciplineR.pdf) were determined in vitro. Both acalabrutinib and ACP‑5862 independently demonstrated low nonspecific binding (3%) to the low-binding polycarbonate tubes and ≥95% stability in mouse, rat, dog, monkey, and human plasma under the assay conditions using LC-MS/MS quantification.

The mean in vitro protein binding ratios of both acalabrutinib (1, 3, and 10 μM) and ACP−5862 (1 and 10 μM) were independent of concentrations tested (Table 1). The plasma protein binding of the acalabrutinib metabolite, ACP‑5862 was consistently higher than acalabrutinib across the mouse, rat, dog, and human plasma tested, with higher binding in rat, relative to other species. The free fraction of ACP-5862 in human plasma was 2-fold lower than acalabrutinib. Acalabrutinib was 93.7% and 41.1% bound in physiologic concentrations of human serum albumin and α1-acid glycoprotein solutions, respectively.

The mean percent distribution of acalabrutinib (1, 3, and 10 µM) and ACP-5862 (1 µM and 10 µM) to blood cells and the calculated blood to plasma ratio were predominantly independent of concentration (Table 2). There was higher plasma-free fraction and greater degree of blood cell partitioning of acalabrutinib in mouse and dog relative to rat and human.

Human Clinical Study Subject Disposition. In cohort 1, all 8 subjects (3 females/5 males; mean ± standard deviation [SD] age: 44 ± 15.2 years) and in cohort 2, all 6 subjects (2 F/4 M; mean ± SD age 38 ± 17.6 years) received study medication. All but 2 subjects, one in each cohort, completed the study. Both subjects withdrew on day 3 for personal reasons, and most PK parameters could be estimated since >90% of radioactivity was excreted at the time of withdrawal. There were no reported adverse events that were greater than Common Terminology Criteria for Adverse Events grade 1.

Human Plasma Pharmacokinetics (Cohort 1, Absolute Bioavailability). The single IV dose of [^{14}C]acalabrutinib ranged from 7.61 to 7.75 µg and the radioactive dose ranged from 961 to 978 nCi. Plasma concentration-time curves following administration of a single oral dose of unlabeled acalabrutinib in its 100 mg to-be-marketed capsule formulation and the [^{14}C]acalabrutinib microtracer administration 58 minutes later as a single IV dose in cohort 1 are shown in Fig. 2, with respective PK parameters summarized in Table 3. The geometric mean exposure ratio (oral/IV) for acalabrutinib dose-normalized area under the concentration time curve from time 0 to infinity ($AUC_{0-\infty}$), as the measure of absolute bioavailability, was 25.3% (CV 14.3%, Table 3). Administration of the IV microtracer dose was within 30 minutes of the median time of maximum observed plasma concentration (T_{max}) for the oral acalabrutinib dose. Oral absorption of acalabrutinib was rapid (T_{max} range, 0.5–0.75 h), and plasma concentrations of acalabrutinib and [^{14}C]acalabrutinib declined in an exponential fashion resulting in similar terminal $t_{½}$ (geometric mean [%CV]) between oral and IV doses; 1.57 (0.60%) h and 1.78 (0.46%) h, respectively. Following the [^{14}C]acalabrutinib IV microtracer dose, total body clearance (CL) was moderate at 39.4 l/h (CV 30.6%) or approximately 45% of liver blood flow; volume of distribution (V_z) was determined to be 98.0 l (CV 42.8%), and apparent V_z at steady state was 34.2 l (CV 40.2%). Less than 2% of the dose was excreted in urine after oral and IV administration. Renal CL (CL_R) of acalabrutinib

DMD Fast Forward. Published on November 15, 2018 as DOI: 10.1124/dmd.118.084459
This article has not been copyedited and formatted. The final version may differ from this version.

following an oral dose (geometric mean cohort 1: 1.21 l/h; cohort 2: 1.33 l/h) accounted for <1% of the apparent total clearance (CL/F) of acalabrutinib in both cohorts. Similarly, CL_R of [^{14}C]acalabrutinib following an IV dose (geometric mean 0.654 l/h; CV 55.6%) accounted for <1% of the CL of [^{14}C]acalabrutinib. Collectively, these data indicate that a minor amount of parent acalabrutinib was eliminated by the renal route.

Blood and Plasma Pharmacokinetics of an Oral [^{14}C]Acalabrutinib Dose in Rat, Dog, and Human

Rat. Acalabrutinib represented 11.3% of the AUC from time 0 to the last quantifiable concentration (AUC_{0-t}) for total radioactivity in male and female rat plasma (Supplemental Table S1). The total radioactivity concentrations observed in whole blood and plasma were similar during the initial absorption and rapid elimination phases through 2 hours postdose (Fig. 3). Then a trend toward increased blood to plasma concentration ratios over time was observed, ranging from a mean of 0.732 to 5.31 for both sexes, which indicated that drug-related radioactivity was increasingly associated with the cellular fraction of blood at later time points. The terminal half-lives calculated for blood were long (215 and 157 hours for male and female, respectively). For plasma, $t_{1/2}$ values were at least 20-fold shorter (10.7 and 4.10 hours for male and female, respectively). There was a sex difference with systemic exposure of drug-related radioactivity, with female animals approximately 40% higher than males.

Dog. Relative to rat, a lower proportion of the dose was metabolized in dog, wherein acalabrutinib represented 45.9% and 41.9% of the AUC_{0-t} total radioactivity in male and female dog plasma, respectively (Supplemental Table S2). The plasma and blood total radioactivity concentration versus time profiles were overlapping (Fig. 3). The elimination half-lives for blood and plasma were short for most animals, with measurable radioactivity observed in all animals through 8 hours postdose, and most animals having

concentrations below the limits of quantification at 24 hours postdose. Systemic exposure was comparable between blood and plasma, and between sexes. Blood:plasma concentration ratios of total radioactivity were consistent from 0.25 to 8 hours postdose, and ranged from a mean of 0.813 to 1.20 for both sexes, indicating that drug-related radioactivity partitioned freely between the plasma and the cellular fraction of blood.

Human (Cohort 2, mass balance). The single oral dose of acalabrutinib ranged from 108.47 to 108.53 mg and the radioactive dose ranged from 994.53 to 995.06 nCi. Plasma concentration-time curves for unlabeled acalabrutinib (LC-MS/MS) and total radioactivity (AMS) are shown in Fig. 3. Like the acalabrutinib parent molecule, total radioactivity in plasma and whole blood revealed rapid absorption after the oral dose (T_{max} range 0.75 to 2 h). Parent acalabrutinib plasma concentrations were a small fraction of the concentrations of total radioactivity and there were no notable sex- or ADME genotype-related PK differences among the 6 individual subjects.

Blood and plasma concentrations of total ^{14}C were similar immediately following the dose and for 12 hours postdose. After reaching C_{max}, total ^{14}C concentrations initially declined rapidly, like acalabrutinib. The parent molecule was measurable only up to 8 hours postdose and had a mean elimination half-life ($t_{1/2}$) value of 1.47 hours. The total ^{14}C in plasma was measurable for 4 days and had a mean terminal $t_{1/2}$ value of 46.5 hours (range 19.6-82.2 h). At 24 hours postdose and later, the total ^{14}C in whole blood was greater than that observed in plasma and was measurable for the 7-day duration of sample collection. The terminal $t_{1/2}$ of these low concentrations of radioactivity in blood ranged from 370 hours to 465 hours; i.e., the estimated terminal $t_{1/2}$ was more than twice as long as the 168-hour sample collection period (n = 5). As in rat, there was also a trend toward an increased blood-to-plasma ratio over time for total radioactivity. The data indicate that small amounts of radioactivity persist in circulation, with an increasing proportion of the remaining radioactivity attributed to the blood cell fraction, relative to plasma.

After a single oral dose of acalabrutinib/[^{14}C]acalabrutinib, the mean ^{14}C radioactivity per million PBMCs, the blood cell fraction containing the target BTK, was highest at 1 hour postdose (0.082 ng eq/million cells) and decreased over time through 48 hours postdose (0.025 ng eq/million cells).

Excretion and Mass Balance.

Rat. Following oral administration of [^{14}C]acalabrutinib to male and female Sprague Dawley rat, the major route of excretion of the administered radioactivity was via the feces (mean 88.3%–91.2%; Table 4). Urinary elimination was minor and there was no obvious sex difference in the rates or routes of excretion. Excretion of the administered radioactivity was rapid, with the majority of the dose recovered in the first 48 hours postdose. Concentrations of radioactivity remaining in the individual carcasses at the end of the collection period (96 hours postdose) ranged from 0.7%–1.0%.

Dog. Following oral administration of [^{14}C]acalabrutinib to Beagle dogs, the major route of excretion of the administered radioactivity was via the feces (mean 69.3%–71.8%, Table 4). Urinary elimination was lower (mean 14.6%–15.2%), and there was no obvious sex difference in the rates or routes of excretion. Excretion of the administered radioactivity was rapid, with most of the dose recovered in the first 48 hours postdose.

Human (Cohort 2). Following a single 100-mg oral dose of acalabrutinib containing a microtracer dose of [^{14}C]acalabrutinib, most total ^{14}C radioactivity was eliminated in the feces (Table 4). Geometric mean recoveries of total radioactivity in urine and feces were 12.0% (min-max range: 10.3%–14.7%) and 83.5% (min-max range: 77.5%–86.9%), respectively. Approximately 96% of total radioactivity was recovered in the excreta; >80% of the total radioactivity was recovered within 96 hours postdose.

Metabolite Profiling. Across multiple in vitro and in vivo preclinical metabolite profiling studies, over three dozen acalabrutinib-related peaks were assigned either via

high-resolution mass defect filtering, or radiochromatographic analysis (data on file). Of these, 15 human and 20 rat and dog metabolite structures were assigned and characterized using a cutoff of >1% of dose (urine and feces) or >1% of AUC (plasma) for the human ADME study. This was based on ^{14}C analysis of time-proportional pooled samples, and a cutoff of >1% of total integrated radioactivity in each radiochromatographic analysis (run) for the rat and dog ADME studies, respectively, in plasma, urine, and feces. Three primary metabolic pathways were characterized, with secondary and tertiary metabolites arising from sequential metabolism and/or combinations of the three major routes (Fig. 1). The three primary metabolic pathways were: amide hydrolysis resulting in loss of the 2-aminopyridine group (M1, ACP-5197, and M2); GSH or cysteine Michael addition to the 2-butynamide moiety to afford novel enol thioether conjugates M5 (ACP-5530) and M10 (ACP-5461), respectively; and pyrrolidine hydroxylation, predominantly at the α-methine carbon of the pyrrolidine ring, to afford active, ring-opened, major circulating metabolite, M27 (ACP-5862). An additional biotransformation pathway was conversion of the warhead alkyne to a β-keto-amide, via hydrolysis of one of the enol thioether conjugates (M23, ACP-5134, Podoll et al., 2018).

Rat plasma. ACP‑5862 (M27) was the major single metabolite in systemic circulation and accounted for 57.4% and 42.1% of the AUC_{0-t} total radioactivity in male and female rat plasma, respectively, approximately 4- to 5-fold higher than parent molecule at 11.3% (Supplemental Table S1, Supplemental Fig. S1). Four additional metabolites, M1 (amide hydrolysis product), M5, M10, and M23 were also detected in rat plasma (Fig. 1), but with lower AUC_{0-t} values that ranged from 4.2%–12.0% of the AUC_{0-t} for total radioactivity in plasma.

Dog plasma. M1, M5, M7/M40 in aggregate, M10, M25, and M27 were detected in dog plasma (Fig. 1), with AUC_{0-t} values that ranged from 1.6%–21.7% of the AUC_{0-t} for

total radioactivity in plasma (Supplemental Table S2, Supplemental Fig. S2). ACP−5862 (M27), the major human metabolite was a relatively minor component in systemic circulation and accounted for 6.1% and 8.1% of the AUC_{0-t} total radioactivity in male and female dog plasma, respectively. In contrast to rat and human, the major circulating metabolites in dog plasma are formed by GSH conjugation of the alkyne moiety of acalabrutinib to afford M5 (GSH conjugate, ACP-5530) and sequential cleavage of M5 to the cysteinyl-glycine (M7, ACP-5531) and cysteine conjugates (M10, ACP-5461). Direct chemical reaction of the 2-butynamide warhead with GSH, Cys-Gly, or Cys is a possible alternative to the GSTM1-mediated formation of the GSH conjugate that was demonstrated in vitro (data on file).

Human plasma. The extraction efficiency of the plasma pools was 85% and the column fraction recovery was 100%. Profiling of ^{14}C showed that acalabrutinib was extensively metabolized (Fig. 4). In time-proportionally pooled human plasma (n = 6), parent acalabrutinib accounted for 8.6% of total radioactivity (Table 5). The most abundant metabolite was M27 (ACP-5862), representing 34.7% of total radioactivity, resulting from primary oxidation of the pyrrolidine ring. M27 was the only single human metabolite representing >10% of radioactivity and was about 4-fold greater than the amount of parent acalabrutinib in the plasma pool. The next most abundant plasma metabolite components after M27 were 10.8% (M7, M8, M9, M10, and M11, collectively), 5.9% (M25), and 2.5% (M3) of radioactivity in the plasma profile. M7, M9, M10, and M11 represent downstream metabolites of GSH conjugation of the 2-butynamide warhead.

Human urine. In mass-proportional pooled human urine (N = 6), parent acalabrutinib accounted for 0.5% of excreted oral dose. The most abundant metabolite cluster co-eluted and was 2.7% of excreted dose, representing mainly M7, M10, and

M11, collectively (Fig. 4). Metabolite M27 (ACP-5862) represented 0.5% of excreted dose.

Human feces. The extraction efficiency of the feces homogenate pools was 89% and the column fraction recovery was 100%. In mass-proportional pooled human feces (*n* = 6), parent acalabrutinib accounted for 1.2% of excreted dose. The most abundant metabolite cluster co-eluted and was 12.1% of excreted dose, representing M22, M45, and M23, collectively (Fig. 4). M23 represents a conversion of the acalabrutinib warhead 2-butynamide to a β-keto-amide (ACP-5134). Empirically, this represents a hydration of the alkyne functional group; however, based on chemical stability, it may be more likely to result from the hydrolysis of enol thioether metabolites in feces (Podoll et al., 2018). Reduction of the ketone of M23 produced the β-hydroxybutanamide M45. The next most abundant feces metabolite components were 7.5%, 5.2%, and 3.5% of excreted dose, representing M24, co-eluting M17 and M18, and M27, respectively. M17 and M24 may result from the further oxidation of M45, and M18 and M22 result from two hydroxylations.

In summary, metabolite profiling and identification data indicate that [^{14}C]acalabrutinib underwent extensive metabolism in humans (Fig. 1, Table 5). This occurred primarily by oxidation of its pyrrolidine ring, with one active metabolite, M27 (ACP-5862), appearing in plasma at an exposure that was higher than parent acalabrutinib. Other pathways involved amide hydrolysis, GSH conjugation, and alkyne hydration. The relatively insignificant excretion of parent acalabrutinib in feces and urine indicates that metabolic clearance is the major route of acalabrutinib elimination in humans.

Discussion

Single oral doses of 100 mg acalabrutinib administered to healthy male and female human subjects in this study were safe and well tolerated. No clinically significant changes or findings were noted from adverse events, clinical laboratory evaluations, vital sign measurements, or 12-lead electrocardiography for this study. Among the male and female subjects enrolled in this study, there was no obvious sex dependence in the PK of acalabrutinib.

In vitro studies established the role of CYP3A and glutathione S-transferase (GSTM1 and GSTM2) in the metabolic turnover of acalabrutinib. In addition, acalabrutinib is a substrate for BCRP. Therefore, the effect of mutations resulting in BCRP (421C>A), CYP3A5 (6986A>G), and GSTM1 (-/- (null), -/+, +/+) on the disposition of acalabrutinib (Lee et al., 2015; Xie et al., 2004; Krivoy et al., 2012) was investigated. Outcomes from the small number of subjects in cohort 2 of this study, coupled with results from several other healthy subject studies (data on file), indicated that an ADME genotype-related impact on acalabrutinib major metabolic clearance pathways was not likely to occur. Given the predominance of the oxidative metabolic pathway, collectively these data indicate that variability in CYP3A4 expression may be the predominant determinant of acalabrutinib exposure in patients.

The absolute bioavailability of acalabrutinib was established using a microtracer approach, wherein the [^{14}C]acalabrutinib IV dose was delivered shortly after the C_{max} for the oral dose of its unlabeled to-be-marketed capsule formulation. Good oral bioavailability (25%) was observed. Rapid absorption of the oral dose was followed by rapid elimination with similar $t_{1/2}$ values between the oral and IV doses. Given the role of CYP3A in the metabolism of acalabrutinib, extraction by gut enzymes during absorption can be anticipated. Concordant with observed bioavailability, acalabrutinib extraction

was approximately 50% for both the gut and the liver (unpublished data) in a Q_{gut} model using IV metabolic clearance data and CYP3A4 scaling from gut to liver (Gertz et al., 2010). By comparison, the first-pass extraction ratio of ibrutinib was estimated to be 92% with low bioavailability (Scheers et al., 2015). High first-pass metabolism appears to contribute to a higher required daily dose to achieve effective BTK target coverage for ibrutinib at 560 mg daily, compared with the 200 mg total daily dose of acalabrutinib in relapsed/refractory mantle cell lymphoma (see IMBRUVICA and CALQUENCE prescribing information).

Acalabrutinib was designed with a less reactive 2-butynamide electrophile to selectively modify cysteine-481 in the ATP binding pocket of BTK by means of an essentially irreversible covalent bond. Ibrutinib binds irreversibly to BTK via a similar mechanism, employing the more reactive acrylamide electrophile, like other approved covalent kinase inhibitors (afatinib, neratinib, and osimertinib). A previous report established increased kinase selectivity of acalabrutinib relative to ibrutinib and spebrutinib, and showed reduced chemical reactivity with GSH in vitro (Barf et al., 2017).

Previous reports of the acrylamide-containing covalent kinase inhibitors have shown significant irreversible binding to off-target proteins (Chandrasekaran et al. 2010; Stopfer et al., 2012; Scheers et al., 2015; Dickinson et al., 2016) that contributed to difficulty measuring the plasma-free fraction in vitro. The reversible plasma protein binding levels of acalabrutinib and ACP-5862 were high and not concentration dependent. The experimental method for noncovalent plasma protein binding studies that was applied to these 2-butynamide covalent inhibitors (acalabrutinib and ACP-5862) indicated recovery and stability consistent with lower binding to off-target proteins than the acrylamide-based TCIs. Acalabrutinib protein binding was lowest in mouse and dog (75.4% and 68.4% bound, respectively), the species with the highest blood cell partitioning (~50% to

56%). In human, plasma protein binding averaged 97.5% and 98.6%, while the blood to plasma ratio averaged 0.79 and 0.66, for acalabrutinib and ACP-5862, respectively. These data indicate that a smaller fraction of the ACP-5862 metabolite total plasma exposure is available for BTK inhibition, relative to the parent molecule. Based on these results, rapid and acceptable recovery of ^{14}C was anticipated during in vivo ADME studies, as little evidence of off-target binding was observed in vitro.

Whole blood and plasma pharmacokinetics for total ^{14}C were very similar in rat, dog, and human during the initial absorption phase. They reached similar C_{max} values and declined rapidly by approximately one log value during the first few hours postdose (Fig. 3). In dog, parent acalabrutinib was a significant proportion of the total radioactivity, accounting for nearly half of the total ^{14}C AUC_{0-t} (Supplemental Table S2). In rat and human, parent acalabrutinib accounted for 11.3% and 8.7% of the AUC_{0-t} for total ^{14}C, indicating greater metabolic clearance, relative to dog. Additionally, during the terminal phase of elimination of ^{14}C in rat and human, a clear trend of increasing blood to plasma ratio was observed as the estimated terminal half-life in the whole blood fraction exceeded the duration of data collection. At the later time points in rat and human >90% and >87% of the administered total radioactivity had been recovered in excreta by 48 and 96 hours postdose, respectively. Measurable amounts of radioactivity persisted in circulation, an increasing proportion of which was observed in the blood cell fraction relative to plasma. This result may be partly attributed to covalent binding of acalabrutinib to its pharmacological target, BTK, which is expressed in components of whole blood. A visual comparison of the relative concentration of residual radioactivity from acalabrutinib versus ibrutinib in human plasma indicates that covalently bound terminal phase residues may be relatively higher in ibrutinib and could be a manifestation of lower butynamide warhead reactivity in acalabrutinib relative to the reactivity of the acrylamide warhead of ibrutinib (Scheers et al., 2015).

Measurement of target engagement in PBMCs via the ^{14}C label was an exploratory objective of the human ADME study. The mean disappearance of ^{14}C in PBMCs across the 6 subjects in cohort 2 was approximately log-linear during the polyexponential elimination from plasma and whole blood (Fig. 3). A portion of the radioactivity observed in the whole blood fraction was confirmed to be associated with PBMCs, the fraction containing the B cells targeted by acalabrutinib therapy. Converting the initial observed ^{14}C concentration in PBMCs to molecules per PBMC resulted in an estimate of approximately 100,000 acalabrutinib molecules per PBMC. It is not clear from these data whether this is a reasonable estimate of BTK content in PBMCs; nonetheless, AMS appears to be (an expensive) potential tool for measuring the elimination of covalently bound BTK from PMBCs, or stated differently, the rate of PBMC BTK resynthesis.

Extrahepatic clearance is a general trait attributed to TCIs based, in part, on the reactivity of the acrylamide electrophile and off-target binding (Shibata and Chiba, 2015; Leung et al., 2017). Given the higher overall 96% recovery of acalabrutinib-related ^{14}C during the human ADME trial, combined with that specifically observed for extraction of feces samples, irreversible protein binding does not appear to be a meaningful route of extrahepatic clearance for acalabrutinib.

The majority of acalabrutinib metabolism could be summarized by three major routes: oxidation of the pyrrolidine ring, GSH conjugation, and amide hydrolysis. Amide hydrolysis is readily quantifiable in rat and dog plasma (M1, Supplemental Tables S1 and S2), but was below quantifiable limits in human plasma, confirmed instead by the downstream metabolite M2. Although the 2-butynamide warhead is retained in this metabolite, the loss of the 2-pyridylbenzamide likely renders it inactive because of lack of affinity for the ATP binding pocket (Barf et al., 2017). Glutathione conjugation of the alkyne moiety of acalabrutinib to afford M5 and sequential cleavage of M5 to the cysteinylglycine (M7) and cysteine conjugates (M10) accounted for a greater proportion

of circulating radioactivity in dog relative to rat and human. Direct chemical reaction with GSH, Cys-Gly, or Cys with the alkyne warhead is possible, yet a screen for acalabrutinib loss suggested an enzymatic requirement for GSTM1 and GSTM2 (data on file).

By far the most abundant metabolite in circulation in rat and human was the oxidation of the pyrrolidine ring resulting in formation of the late-eluting, active metabolite M27 (ACP-5862). In vitro BTK inhibition experiments with acalabrutinib and ACP-5862 showed covalent inhibition by both, determined K_I and k_{inact} values, and demonstrated similar kinase selectivity profiles (In preparation, Podoll et al., 2018). The percent of plasma AUC in human, as determined by time-proportional pooling was 34.7% of the total radioactivity in circulation, 4 times greater than parent acalabrutinib (8.6%). No other metabolites were greater than 10% of circulating radioactivity. Detailed metabolite structure elucidation studies were conducted to discern the site of oxidation and final structure of the late-eluting metabolite ACP-5862 (In preparation, Podoll et al., 2018).

The β-ketoamide, M23 (ACP-5134, also a known degradation product of acalabrutinib [data on file]), made up a large proportion of the radioactivity excreted in feces (Fig. 4 and Table 5). Chemical hydration of the acalabrutinib butynamide warhead in vitro to directly afford ACP-5134 is slow (data on file), and ACP-5134 levels in human plasma are low. The relatively high plasma concentrations of novel enol thioether conjugates (M5, M7, and M10) arising from Michael addition of thiols to the acalabrutinib warhead, led to stability studies on the synthetic standard of M5 (ACP-5530). Results showed that enol thioether metabolites are potential precursors of β-ketoamide-derived metabonates in feces (In preparation, Podoll et al., 2018).

Relative to acrylamide-containing TCIs previously approved by the FDA, acalabrutinib is less GSH-reactive, and this may account for acalabrutinib's BTK

selectivity and lower off-target binding in plasma in this human ADME study. Acalabrutinib's moderate hepatic oxidative metabolic clearance to an active circulating metabolite, coupled with good oral absolute bioavailability that results in high and sustained BTK occupancy in lymphoma patients dosed with a 100 mg twice daily regimen, all indicate suitable PK for a short half-life covalent agent with extended biologic activity against BTK.

Acknowledgments

The authors thank Christine Hale, MD (Covance, Principal Investigator); Brett Pick (Covance, preparation of the clinical doses); Gina Patel (Covance, pharmacokinetic analysis); Elizabeth Spencer (Covance, nonclinical ADME); Bioanalytical Systems, Inc. (BASi, acalabrutinib clinical sample bioanalysis); Cancer Genetics, Inc. (CGI, ADME genotyping); Teresa Middleton and Savannah Varney (Covance, PBMC isolation); Michael Gulrajani and Jean Cheung (Acerta Pharma, PBMC preparation); and Beverly Stanley, ELS (Team 9 Science, LLC, editorial support).

Authorship Contributions

Participated in research design: Podoll, Pearson, Evarts, Ingallinera, Bibikova, Slatter.

Conducted experiments: Ingallinera, Sun, Gohdes, Sanghvi.

Performed data analysis: Podoll, Evarts, Ingallinera, Sun, Gohdes, Cardinal, Slatter, Sanghvi.

Wrote or contributed to writing of manuscript: Podoll, Pearson, Slatter.

References

Baillie T (2016) Targeted covalent inhibitors for drug design. *Angew Chem Int Ed* **55**:13408-13421.

Barf T and Kaptein A (2012) Irreversible protein kinase inhibitors: balancing the benefits and risks. *J Med Chem* **55**:6243–6262.

Barf T, Covey T, Izumi R, van de Kar B, Gulrajani M, van Lith B, van Hoek M, de Zwart E, Mittag D, Demont D, Verkaik S, Krantz F, Pearson PG, Ulrich R, and Kaptein A (2017) Acalabrutinib (ACP-196): a covalent Bruton tyrosine kinase (BTK) inhibitor with a differentiated selectivity and in vivo potency profile. *J Pharmacol Exp Ther* **363**:240–252.

Buggy JJ and Elias L (2012) Bruton tyrosine kinase (BTK) and its role in B-cell malignancy. *Int Rev Immunol* **31**:119–132.

Byrd JC, Harrington, B, O'Brien S, Jones JA, Schuh A, Devereux S, Chaves J, Wierda WG, Awan FT, Brown, JR Hillmen P, Stephens DM, Ghia P, Barrientos JC, Pagel JM, Woyach J, Johnson D, Huang J, Wang X, Kaptein A, Lannutti, BJ, Covey T, Fardis M, McGreivy J, Hamdy A, Rothbaum W, Izumi R, Diacovo TG, Johnson AJ, and Furman RR (2016) Acalabrutinib (ACP-196) in relapsed chronic lymphocytic leukemia. *N Engl J Med* **374**: 323–332.

Chandrasekaran A, Shen L, Lockhead S, Oganesian A, Wang J, and Scatina J (2010) Reversible covalent binding of neratinib to human serum albumin in vitro. *Drug Metab Lett* **4**:220–227.

Dickinson PA, Cantarini MV, Collier J, Frewer P, Martin S, Pickup K, and Ballard P (2016) Metabolic disposition of osimertinib in rats, dogs, and humans: insights into a drug designed to bind covalently to a cysteine residue of epidermal growth factor receptor. *Drug Metab Dispos* **44**:1201–1212.

Gertz M, Harrison A, Houston JB, and Galetin A (2010) Prediction of human intestinal first-pass metabolism of 25 CYP3A substrates from in vitro clearance and permeability data. *Drug Metab Dispos* **38**:1147–1158.

Hamilton RA, Garnett WR, and Kline BJ (1981) Determination of mean valproic acid serum level by assay of a single pooled sample. *Clin Pharmacol Ther* **29**:408–413.

Krivoy N, Zuckerman T, Elkin H, Froymovich L, Rowe JM, and Efrati E (2012) Pharmacokinetic and pharmacogenetic analysis of oral busulfan in stem cell transplantation: prediction of poor drug metabolism to prevent drug toxicity. *Current Drug Safety* **7**:211–217.

Lappin G and Stevens L (2008) Biomedical accelerator mass spectrometry: recent applications in metabolism and pharmacokinetics. *Expert Opin Drug Metab Toxicol* **4**:1021–1033.

Lee CA, O'Connor MA, Ritchie TK, Galetin A, Cook JA, Ragueneau-Majlessi I, Ellens H, Feng B, Taub ME, Paine MF, Polli JW, Ware JA, and Zamek-Gliszczynski MJ (2015) Breast cancer resistance protein (ABCG2) in clinical pharmacokinetics and drug interactions: practical recommendations for clinical victim and perpetrator drug-drug interaction study design. *Drug Metab Dispos* **43**:490–509.

Leung L, Yang X, Strelevitz TJ, Montgomery J, Brown MF, Zientek MA, Banfield C, Gilbert AM, Thorarensen A, and Dowty ME (2017) Clearance prediction of targeted covalent inhibitors by in vitro-in vivo extrapolation of hepatic and extrahepatic clearance mechanisms. *Drug Metab Dispos* **45**:1–7.

Liu Q, Sabnis Y, Zhao Z, Zhang T, Buhrlage SJ, Jones LH, Gray NS (2013) Developing irreversible inhibitors of the protein kinase cysteinome. *Chem & Biol* **20**:146–159.

Lonsdale R and Ward RA (2018) Structure-based design of targeted covalent inhibitors *Chem Soc Rev* **47**:3816–3830.

Moghaddam MF, Tang Y, O'Brien Z, Richardson SJ, Bacolod M, Chaturvedi P, Apuy J, and Kulkarni A (2014) A proposed screening paradigm for discovery of covalent inhibitor drugs. *Drug Metab Lett* **8**:19–30.

Podoll T, Pearson PG, Kaptein A, Evarts J, Ingallinera T, Sun H, Byard SJ, and Slatter, JG (2018). Structure elucidation, metabolism, drug interaction potential, and preclinical pharmacologic profile of ACP-5862, the major, circulating, active metabolite of the covalent BTK inhibitor, acalabrutinib. Manuscript in Preparation.

Ponader S, and Burger JA (2014) Bruton's tyrosine kinase: from X-linked agammaglobulinemia toward targeted therapy for B-cell malignancies. *J Clin Oncol* **32**:1830–1839.

Sarapa N, Hsyu P-H, Lappin G, and Garner RC (2005) The application of accelerator mass spectrometry to absolute bioavailability studies in humans: simultaneous administration of an intravenous microdose of ^{14}C-nelfinavir mesylate solution and oral nelfinavir to healthy volunteers. *J Clin Pharmacol* **45**:1198–1205.

Scheers E, Leclercq L, de Jong J, Bode N, Bockx M, Laenen A, Cuyckens F, Skee D, Murphy J, Sukbuntherng J, and Mannens G (2015) Absorption, metabolism, and excretion of oral ^{14}C radiolabeled ibrutinib: An open-label, phase 1, single-dose study in healthy men *Drug Metab Dispos* **43**:289–297.

Shibata Y and Chiba M (2015) The role of extrahepatic metabolism in the pharmacokinetics of the targeted covalent inhibitors afatinib, ibrutinib, and neratinib. *Drug Metab Dispos* **43**:375–384.

Singh J, Petter RC, Baillie TA, and Whitty A, (2011) The resurgence of covalent drugs. *Nat Rev Drug Discov* **10**:307–317.

Stopfer P, Marzin K, Narjes H, Gansser D, Shahidi M, Uttereuther-Fischer M, and Ebner T (2012) Afatinib pharmacokinetics and metabolism after oral administration to healthy male volunteers. *Cancer Chemother Pharmacol* **69**:1051–1061.

Wang M, Rule S, Zinzani PL, Goy A, Casasnovas O, Smith SD, Damaj G, Doorduijn J, Lamy T, Morschhauser F, Panizo C, Shah B, Davies A, Eek R, Dupuis J, Jacobsen E, Kater AP, Le Gouill S, Oberic L, Robak T, Covey T, Dua R, Hamdy A, Huang X, Izumi R, Patel P, Rothbaum W, Slatter JG, and Jurczak W (2018) Acalabrutinib in relapsed or refractory

mantle cell lymphoma (ACE-LY-004): a single-arm, multicenter, phase 2 trial. *The Lancet* **391**:659–667.

Xie HG, Wood AJ, Kim RB, Stein CM, and Wilkinson GR (2004) Genetic variability in CYP3A5 and its possible consequences. *Pharmacogenomics* **5**:243–272.

Zhao Z and Bourne PE (2018) Progress with covalent small-molecule kinase inhibitors. *Drug Discov Today* **23**:727–735.

Footnotes

This work was supported by Acerta Pharma, and has not been previously presented.

Reprint requests should be sent to Terry Podoll, PhD, Principal, IV/PO, LLC, 5021 Bowen Place South, Seattle, WA 98118-2336 or terry.podoll@iv-po.com.

Figure Legends

Fig. 1. Proposed metabolic pathways of acalabrutinib.

Fig. 2. Arithmetic mean (S.D.) logarithmic-linear concentration-time profiles for intravenous [^{14}C]acalabrutinib and oral unlabeled acalabrutinib in plasma (Cohort 1)

Fig. 3. Arithmetic mean (S.D.) logarithmic-linear concentration-time profiles for (A) rat total ^{14}C in blood and plasma and acalabrutinib in plasma of male and female rats; (B) dog total ^{14}C in blood and plasma and acalabrutinib in plasma of overall dogs; and (C) human total ^{14}C in blood, plasma, and PBMCs, and acalabrutinib in plasma (Cohort 2). PBMC, peripheral blood mononuclear cell.

Fig. 4. Reconstructed accelerator mass spectrometry (AMS) chromatograms from plasma extract (A), urine (B), and feces extract (C) following a single oral administration of [^{14}C]acalabrutinib (100 mg, 1 μCi) to healthy male and female subjects showing metabolites identified in each matrix. AUC, area under the plasma concentration-time curve.

DMD Fast Forward. Published on November 15, 2018 as DOI: 10.1124/dmd.118.084459
This article has not been copyedited and formatted. The final version may differ from this version.

Tables.

TABLE 1

Mean reversible protein binding of [^{14}C]acalabrutinib (1, 3 or 10 μM) and ACP-5862 (1 or 10 μM) in mouse, rat, dog, and human plasma and human serum albumin and α1-acid glycoprotein in vitro by ultracentrifugation

Species	**Acalabrutinib**		**ACP‑5862**	
	Bound (%)	**Unbound (%)**	**Bound (%)**	**Unbound (%)**
Mouse	75.4	24.6	98.6	1.4
Rat	92.0	8.0	99.8	0.2
Dog	68.4	31.6	94.3	5.7
Human	97.5	2.5	98.6	1.4
HSA	93.7	6.3	ND	ND
AGP	41.1	58.9	ND	ND

Abbreviations: AGP, acid glycoprotein; HSA, human serum albumin; ND, not determined.

TABLE 2

Mean blood cell partitioning of acalabrutinib (1, 3, or 10 μM) and ACP-5862 (1 or 10 μM) incubated in mouse, rat, dog, monkey and human whole blood in vitro

Species	**Acalabrutinib**		**ACP‑5862**	
	Distribution into blood cells (%)	**Blood to plasma ratio**	**Distribution into blood cells (%)**	**Blood to plasma ratio**
Mouse	56.2	1.37	23.3	0.87
Rat	29.6	0.87	73.7	2.54
Dog	49.6	1.06	67.4	1.40
Human	26.4	0.79	11.6	0.66

TABLE 3

Summary of geometric mean (%CV) pharmacokinetic parameters of acalabrutinib and total ^{14}C radioactivity in healthy human subjects following 100 mg oral, and ≤10 µg IV doses

	Geometric Mean (%CV)				
	Acalabrutinib	[^{14}C]Acalabrutinib[a]	Acalabrutinib	Total ^{14}C[b]	
Parameter	Oral Dose Cohort 1	IV Dose Cohort 1	Plasma Cohort 2	Plasma Cohort 2	Whole Blood Cohort 2
	(*n* = 8)	(*n* = 8)	(*n* = 6)	(*n* = 6)	(*n* = 6)
C_{max} (ng/ml)	639 (53.8)	510 (56.3)	305 (44.0)	1340 (34.4)	1060 (31.3)
T_{max} (h)[c]	0.50 (0.50–0.75)	0.075 (0.033–0.117)	0.5 (0.5–0.517)	0.875 (0.750–2.00)	0.750 (0.750–2.00)
$AUC_{0\text{-}t}$ (ng•h/ml)	643 (39.7)	201 (32.6)	386 (39.2)	5930 (29.4)	11500 (27.1)
$AUC_{0\text{-}12h}$ (ng•h/ml)	642 (35.9)	199 (30.2)	406 (36.6)	4390 (29.4)	3760 (29.6)
$AUC_{0\text{-}168h}$ (ng•h/ml)	ND	ND	407 (36.6)	6250 (24.9)	11500 (27.1)
$AUC_{0\text{-}\infty}$ (ng•h/ml)	643 (35.7)	199 (30.2)	407 (36.6)	6410 (25.1)	ND
$t_{1/2}$ (h)	1.57 (0.600)	1.78 (0.461)	1.47 (0.45)	46.5 (21.8)	395 (9.6)[d]
CL or CL/F (l/h)	163 (35.7)	39.4 (30.6)	246 (36.6)	ND	ND
V_z or V_z/F (l)	344 (36.2)	98.0 (42.8)	499 (36.1)	ND	ND
V_{ss} (l)	ND	34.2 (40.2)	ND	ND	ND
F (%)[e]	25.3 (14.3)	NA	NA	NA	NA

TABLE 3

Summary of geometric mean (%CV) pharmacokinetic parameters of acalabrutinib and total ^{14}C radioactivity in healthy human subjects following 100 mg oral, and ≤10 µg IV doses

	Geometric Mean (%CV)				
	Acalabrutinib	[^{14}C]Acalabrutinib[a]	Acalabrutinib	Total ^{14}C[b]	
Parameter	Oral Dose Cohort 1	IV Dose Cohort 1	Plasma Cohort 2	Plasma Cohort 2	Whole Blood Cohort 2
	(*n* = 8)	(*n* = 8)	(*n* = 6)	(*n* = 6)	(*n* = 6)
Acalabrutinib:Total ^{14}C $AUC_{(0-\infty)}$ ratio	ND	ND	NA	0.0635 (17.8)	NA
CL_R (l/h)	1.21 (32.8)	0.654 (55.6)	1.33 (36.0)	ND	ND
Cumulative $\%f_{eu}$ (%)	0.759 (28.3)	1.69 (45.7)	0.519 (56.5)	ND	ND

TABLE 3

Summary of geometric mean (%CV) pharmacokinetic parameters of acalabrutinib and total ^{14}C radioactivity in healthy human subjects following 100 mg oral, and ≤10 µg IV doses

	Geometric Mean (%CV)				
	Acalabrutinib	[^{14}C]Acalabrutinib[a]	Acalabrutinib	Total ^{14}C[b]	
Parameter	Oral Dose Cohort 1	IV Dose Cohort 1	Plasma Cohort 2	Plasma Cohort 2	Whole Blood Cohort 2
	(*n* = 8)	(*n* = 8)	(*n* = 6)	(*n* = 6)	(*n* = 6)

Abbreviations: $AUC_{0\text{-}12h}$, area under the plasma concentration-time curve from 0 hour to 12 hours; $AUC_{0\text{-}168h}$, AUC from 0 hour to 168 hours; $AUC_{0\text{-}\infty}$, AUC from 0 hour to infinity; C_{max}, maximum observed plasma concentration; CL, total body clearance; CL_R, renal clearance; CV, coefficient of variation; F, bioavailability fraction of dose absorbed relative to IV dosing expressed as a percent; Cumulative $\%f_{eu}$, cumulative percent excreted in urine over the entire sample collection period; IV, intravenous; NA/ND, not applicable or not determined; T_{max}, time of maximum observed plasma concentration; $t_{1/2}$, terminal half-life; V_{ss}, volume of distribution at steady state; V_z, volume of distribution at steady state.

[a] Units are (pg-eq./ml) or (pg-eq.• h/ml).

[b] Units are (ng-eq./ml) or (ng-eq.• h/ml).

[c] Median (min-max).

[d] *n* = 5, half-life value is greater than 2 times the sampling interval.

[e] Absolute bioavailability was calculated using dose normalized $AUC_{0\text{-}\infty}$ following oral and IV administration due to differing doses with each route of administration using the equation F = [$AUC_{0\text{-}\infty}$ (oral)/ $AUC_{0\text{-}\infty}$ (IV)]/Dose (IV)/Dose (oral)].

TABLE 4

Summary of mean (± SD) total recovery of radioactivity 0-96 hours after an oral dose of [^{14}C]acalabrutinib to male and female rats and dogs; and geometric mean (%CV) 0-168 hours after an oral dose to male and female human subjects expressed as a percentage of administered dose

Type of Sample	**Percentage of Administered Dose Recovered**				
	Rat		**Dog**		**Human**
	Male (*n* = 3)	**Female (*n* = 3)**	**Male (*n* = 3)**	**Female (*n* = 3)**	**Overall (*n* = 6)**
Urine	2.7 ± 0.8	3.6 ± 0.3	15.2 ± 1.4	14.6 ± 3.0	12.0 (15.9)
Feces	91.2 ± 6.0	88.3 ± 3.6	71.8 ± 0.7	69.3 ± 7.9	83.5 (5.1)
Cage rinse	0.2 ± 0.03	0.8 ± 0.4	2.5 ± 0.9	1.6 ± 1.9	N/A
Carcass	0.7 ± 0.1	1.0 ± 0.5	N/A	N/A	N/A
Total	96.8 ± 3.5	94.3 ± 2.6	91.1 ± 0.5	87.5 ± 6.3	95.7 (4.5)

TABLE 5

Acalabrutinib metabolites identified in human plasma, urine, and feces

Component	Proposed identification	rt (min)	m/z (mass/charge)	% of Excreted Dose		% of AUC
				Human feces	Human urine	Human plasma
M2	Oxidation, amide hydrolysis	11.3[a]	406.1506	Trace	Trace	ND
M3	Oxidation, dealkylation	17.2[a]	431.1459	1.8	1.3	2.5
M37	$[M + H]^+ = 442$	22.1[a]	442.1983	Trace	Trace	ND
M5 (ACP-5530)	Glutathione adduct	24.3[b]	773.2808	ND	ND	2.2
M7 (ACP-5531)	Cysteinylglycine adduct	27.6[b]	644.2381	ND	2.7	10.8
M9	Oxidized ACP-5531	27.7[b]	660.2328	ND		
M10 (ACP-5461)	Cysteine adduct	28.1[b]	587.2178	Trace		
M11	Oxidized ACP-5461	28.3[a]	603.2129	Trace		
M14 (ACP-5825)	Oxidation (pyrrolidine)	29.5[a]	482.1928	Trace	Trace	ND
M16	Reduction of M27	30.9[a]	484.2088	2.9	0.6	2.2

TABLE 5

Acalabrutinib metabolites identified in human plasma, urine, and feces

Component	Proposed identification	rt (min)	m/z (mass/charge)	% of Excreted Dose		% of AUC
				Human feces	Human urine	Human plasma
M17	Reduced ACP-5134, pyrrolidine oxidation and dehydration	31.6[a]	484.2087	5.2	Trace	ND
M18	Two oxidations (+O_2)	31.4[c]	498.1879		ND	Trace
M22	Two oxidations (+O_2)	33.0[a]	498.1878	12.1	0.5	Trace
M45	Reduced ACP-5134	33.0[c]	486.2242		Trace	Trace
M23 (ACP-5134)	Hydrated alkyne	33.6[a]	484.2086		Trace	Trace
M24	Reduced ACP-5134 +O	34.2[a]	502.2192	7.5	Trace	Trace
M25	Oxidation (pyrrolidine), dehydration	35.6[a]	464.1825	Trace	0.2	5.9
Parent	Acalabrutinib	38.5[b]	466.1983	1.2	0.5	8.6

TABLE 5

Acalabrutinib metabolites identified in human plasma, urine, and feces

Component	Proposed identification	rt (min)	m/z (mass/charge)	% of Excreted Dose		% of AUC
				Human feces	Human urine	Human plasma
M27 (ACP‑5862)	Oxidation (pyrrolidine), ring opening	41.6[b]	482.1935	3.5	2.5	34.7

Abbreviations: AUC, area under the concentration time curve; rt, retention time.

Note: a, b, and c indicate retention times from human urine, plasma, or feces chromatograms, respectively. Grouped metabolites co-eluted in the same fractions comprising the reconstructed chromatographic trace.

Trace = component was observed via MS/MS, but ^{14}C was not above baseline; ND = not detected.

Figures.

Fig. 1.

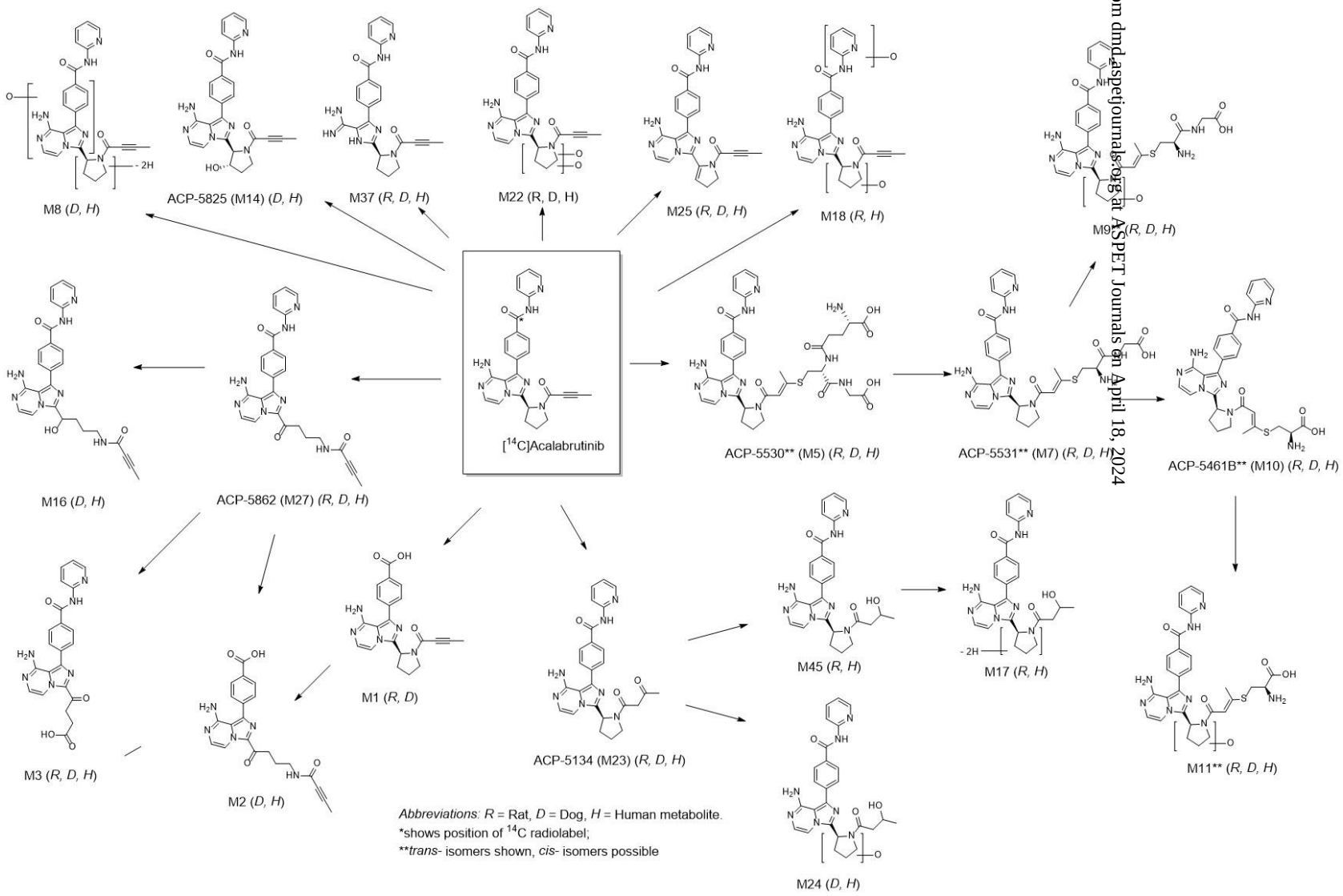

DMD Fast Forward. Published on November 15, 2018 as DOI: 10.1124/dmd.118.084459
This article has not been copyedited and formatted. The final version may differ from this version.

Fig. 2.

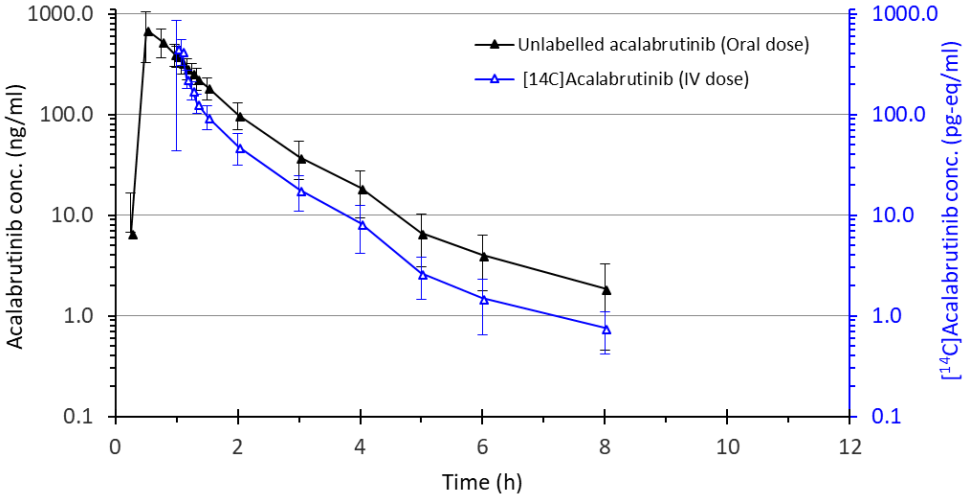

Abbreviation: IV, intravenous.

DMD Fast Forward. Published on November 15, 2018 as DOI: 10.1124/dmd.118.084459
This article has not been copyedited and formatted. The final version may differ from this version.

Fig. 3.

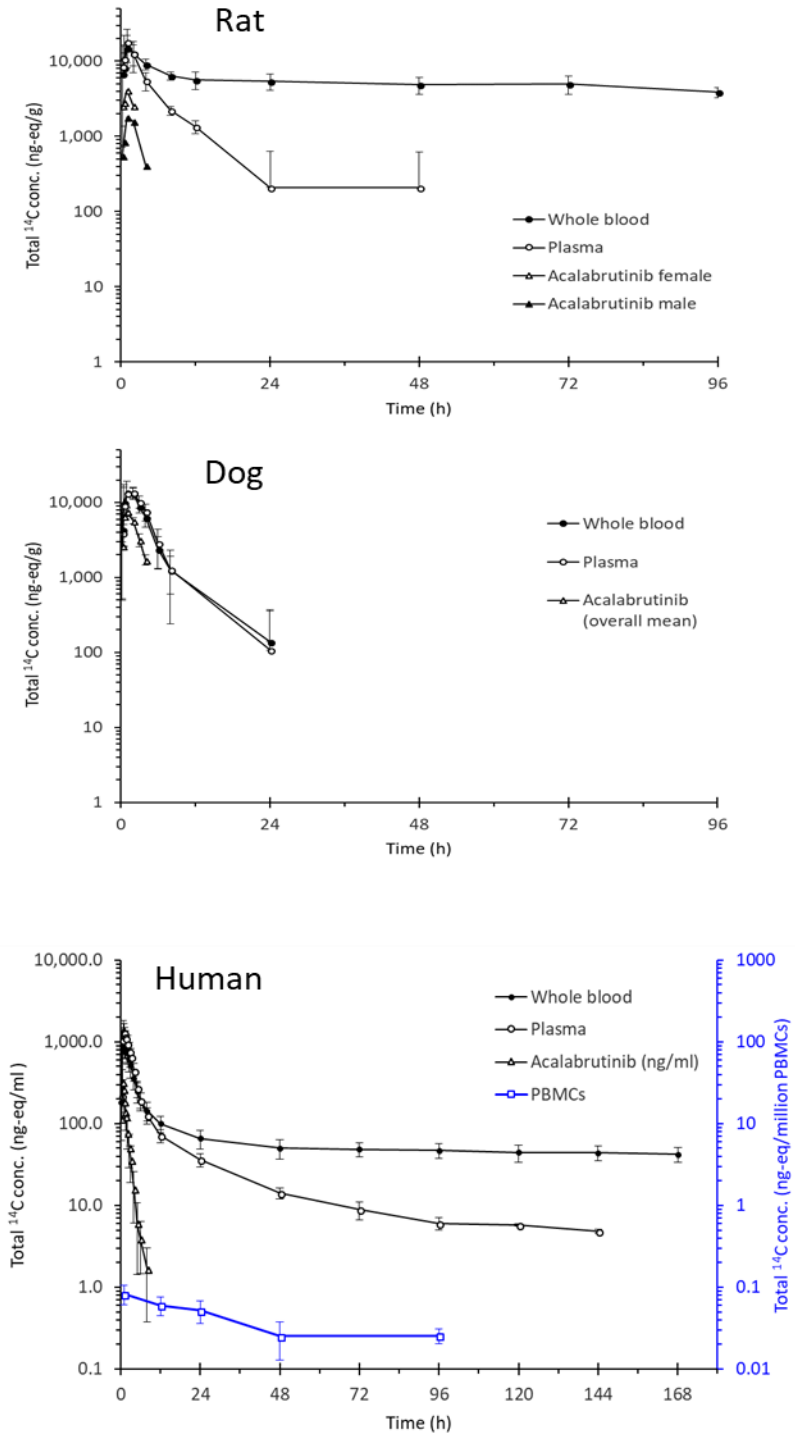

DMD Fast Forward. Published on November 15, 2018 as DOI: 10.1124/dmd.118.084459
This article has not been copyedited and formatted. The final version may differ from this version.

Fig. 4.